Electronic properties of CdSe nanocrystals in the absence and presence of a dielectric medium

Eran Rabani, Balázs Hetényi, and B. J. Berne
Department of Chemistry and Center for Biomolecular Simulation, Columbia University, 3000 Broadway, New York, New York 10027

L. E. Brus
Department of Chemistry, Columbia University, 3000 Broadway, New York, New York 10027

(Received 16 October 1998; accepted 8 December 1998)

We present a detailed study of the electronic properties of CdSe nanocrystals in the absence and presence of a dielectric medium. The electronic structure of the nanocrystal is modeled within the framework of the empirical pseudopotential method. We use a real-space grid representation of the wave function, and obtain the eigenvalues and eigenstates of the one-electron Hamiltonian using a slightly modified version of the filter-diagonalization method. The band gap, density of states, charge density, multipole moments, and electronic polarizabilities are studied in detail for an isolated nanocrystal. We discuss the implications of the results for the long range electrostatic and dispersion interactions between two CdSe nanocrystals. To study the effects of the surroundings we develop a self-consistent reaction field method consistent with the empirical pseudopotential method. We use the eigenstates of the isolated nanocrystal and iterate the self-consistent equations until converged results are obtained. The results show that the electronic properties of polar CdSe nanocrystals are quite sensitive to the environment. © *1999 American Institute of Physics.* [S0021-9606(99)70910-4]

I. INTRODUCTION

The interest in semiconductors which are spatially confined to a few tens of nanometers, and which contain hundreds of atoms, has increased in recent years.[1–9] The development of experimental methods along with improvements in epitaxial growth techniques,[10–13] has made it possible to study various electronic properties of semiconductor nanocrystals in great detail. In particular colloidally prepared CdSe nanocrystals have received much of the experimental attention.[10,11,14–26] The experimental interest in CdSe nanocrystals has raised a number of questions that require the use of electronic structure theory for a complete explanation. Exact electronic structure calculations of CdSe nanocrystals are extremely difficult in view of the large number of atoms and electrons involved,[27] and the lack of periodicity. Therefore, several approximate theoretical methods and models have been developed in the last few years. The simplest approach is based on the effective mass approximation,[28–31] which can be extended to incorporate multiband couplings,[32] i.e., band mixing induced by the effect of finite size.[23,33–36] Another approach is based on the widely used tight binding model,[37] where explicit atomic structure of the nanocrystals is considered.[38–42] A third approach is based on the empirical pseudopotential method,[43] and is the one we adopt in the present study. The pseudopotential method has been applied to a variety of semiconductor nanocrystals at different levels of approximation, and has provided excellent agreement with experimental results.[44–67]

Most theoretical studies have focused on the absorption spectrum of isolated nanocrystals, and neglected the interaction of the nanocrystals with the environment. However, since CdSe nanocrystals are typically deposited on thin films or embedded in glassy materials, it is important to understand the effects of the surroundings on the electronic properties. This is the main goal of the present study. Motivated by the work of Brus[29,68] who treated the solvation of nanocrystals using both a classical dielectric continuum model and an effective mass approximation, we develop a model for the electronic structure of a CdSe nanocrystal which is based on the empirical pseudopotential method,[43] and study the solvation of nanocrystals within the reaction field continuum model.[69–71] Our treatment is different from the effective mass approximation in that we explicitly consider the molecular structure of the nanocrystal, and we describe the solvation of the nanocrystal quantum mechanically.

In Sec. II we provide the details of our model, which include the direct empirical pseudopotential method and the self-consistent reaction field method. We first describe the construction of the empirical pseudopotential suitable for the finite size calculations of CdSe nanocrystals along with the details of the surface passivation. Next, we describe the filter-diagonalization method[72–76] and introduce some modifications. The filter-diagonalization method is used to obtain the eigenstates and eigenvalues of the screened one-electron Hamiltonian, and as far as we know, this is the first study of electronic structure using this method. The last part of this section is devoted to the development of a self-consistent reaction field method consistent with the empirical pseudopotential method.

The electronic properties of isolated CdSe nanocrystals are discussed in Sec. III. We study the density of states and the band gap of a nanocrystal in the strong confinement re-

gime, with diameters ranging from 15 to 50 Å. The electronic properties are then discussed in terms of electronic charge densities, multipole moments, and polarizabilities. The long range electrostatic and dispersion interaction between nanocrystals are directly related to these properties.

The influence of a dielectric medium outside the nanocrystal is discussed in Sec. IV for collective and single state properties. We also discuss the effects of an excess electron in a CdSe nanocrystal which is assumed to occupy the lowest unoccupied molecular orbital (LUMO) state. A summary of the results is given in Sec. V.

II. MODEL AND METHODS

In this section we provide the details of the numerical calculations. First, we describe the pseudopotential for CdSe and the modifications needed in the study of CdSe nanocrystals, including the passivation of the surface. Next we outline the method we use to obtain the eigenstates and eigenvalues of the screened one-electron Hamiltonian. Finally, we develop a reaction field method consistent with the empirical pseudopotential method. Throughout, the following notation is used: A vector is denoted by a bold face, an operator by a hat, and a matrix by a tilde.

A. The direct pseudopotential method

The use of empirical pseudopotential methods to calculate the electronic structure of semiconductor nanocrystals has been very fruitful. Ramakrishna *et al.* have introduced the truncated crystal method,[44–50] in which the bulk empirical Hamiltonian is diagonalized using several bulk Bloch wave functions, and the energy levels of the nanocrystals are obtained by imposing appropriate boundary conditions on the wave functions. Mizel and Cohen[65–67] have introduced a Wannier function approach, in which the electronic properties of a nanocrystal are described in terms of several localized Wannier wave functions. Unlike the truncated crystal method which imposes the boundary conditions in momentum space (e.g., only allowed k states which correspond to standing waves in the sphere are used), the Wannier function approach uses the real space positions of the atoms to describe the boundary of the nanocrystal. Both methods assume an infinite potential outside the core region, which simplifies the numerical calculations, but this approach is not appropriate when a continuum dielectric model of the solvent is introduced. Zunger and collaborators have developed a direct molecular method,[51–64] which is the one we adopt in the present work. The direct method has been used to predict quantum confinement effects, such as the size dependent band gap, and the exciton Coulomb and exchange energies.[51–64]

The direct molecular method starts from a microscopic one-electron Hamiltonian, however, since a full *ab initio* calculation is impractical, the Hamiltonian is simplified, and the exact total screened potential is replaced by a superposition of empirical atomic pseudopotentials. The one-electron Hamiltonian takes the form (in atomic units)

$$\hat{H} = -\tfrac{1}{2}\hat{\nabla}^2 + \sum_{\alpha} V_{\alpha}(|\hat{\mathbf{r}} - \mathbf{R}_{\alpha}|) + \sum_{\beta} V_{\beta}^{\text{ligand}}(|\hat{\mathbf{r}} - \mathbf{S}_{\beta}|), \quad (1)$$

where $\mathbf{R}_{\alpha}$ is the position of atom α, and the index α runs over all atoms. V_{α} is the effective pseudopotential of atom α (i.e., Cd or Se atoms), which is adjusted to fit experimental or *ab initio* data. The last term represents the ligand potentials used to passivate the surface atoms, where the index β runs over all the ligand sites defined below.

In the present work we construct an empirical pseudopotential based on the traditional Bergstresser and Cohen local empirical pseudopotential for CdSe.[77] We use a local potential to minimize the computational effort required to incorporate the effects of the surroundings (the Hamiltonian with the local potential has a smaller energy range compared to the Hamiltonian with a nonlocal potential). The local potential is well known to underestimate the band dispersion and is inadequate in reproducing the shallow d-band in Cd.[43] Nevertheless, it provides qualitative agreement with experiments[43] and thus is sufficient to provide a qualitative description of the effects of the surroundings.

In the classic empirical pseudopotential methods,[43,78] the pseudopotential is defined only on the discrete bulk reciprocal lattice vectors. However, to properly describe a nanocrystal, one needs a continuous potential because of the breakdown of translational symmetry. For precisely this reason, we use the following functional form (in momentum space $\mathbf{q}$) for Cd and Se pseudopotentials

$$V(\mathbf{q}) = a_1(q^2 - a_2)/(a_3 \exp(a_4 q^2) + 1), \quad (2)$$

where $q = |\mathbf{q}|$. This form has been used in the study of the electronic structure of semiconductor surfaces[79,80] and of silicon nanocrystals.[51]

We fit the parameters $a_j\,(j = 1-4)$ to the bulk band structure obtained from the Bergstresser and Cohen empirical pseudopotential[77] for both hexagonal and zincblende crystal structures. The results are shown in Fig. 1, and the agreement between the two calculations for the band structure is very good. The parameters for both crystal structures are given in Table I. Since the fits involve only eight parameters, it is rather straightforward to efficiently sample the relevant range of parameters.[81] Using our new pseudopotential we find that the band gap for the hexagonal crystal structure is 1.82 eV (1.80 eV using Bergstresser and Cohen empirical pseudopotential), and for the zincblende crystal structure is 1.81 eV (1.84 eV using Bergstresser and Cohen empirical pseudopotential). Both results lie near the experimental value of 1.74 ± 0.1 eV for the hexagonal crystal structure.[82] We note that the treatment of the spin–orbit interactions in our model is the same as in the work of Bergstresser and Cohen.[77]

The pseudopotentials are shown in Fig. 2 along with the discrete values of Bergstresser and Cohen.[77] The value of the Cd and Se potentials at $q = 0$ only determines the offset of the bands for bulk calculations and not the spacings between the levels. For this reason, their values were not given in the original work of Bergstresser and Cohen.[77] The results (symbols) shown for $q = 0$ are obtained from the experimental work function[83] which equals the sum of the two potentials at $q = 0$, along with the value of the difference between the Cd and Se potentials at $q = 0$ taken from the local part of the Wang and Zunger semiempirical potential.[83]

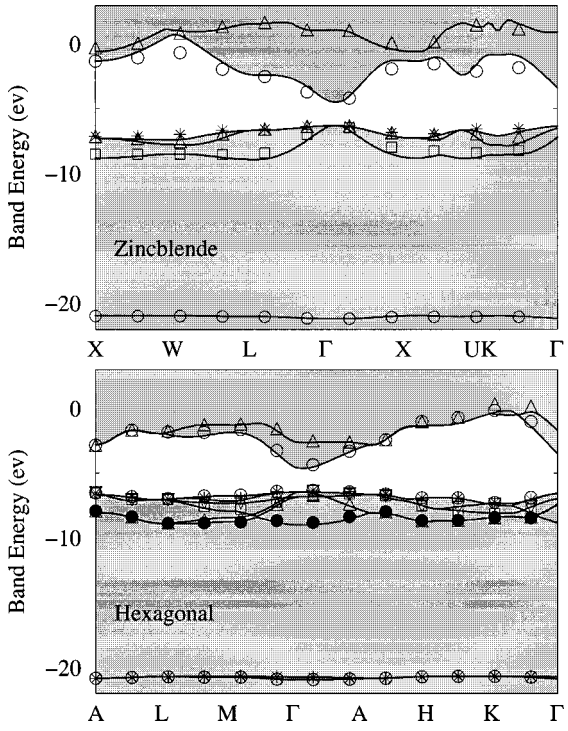

FIG. 1. The band structure of hexagonal (lower panel) and zincblende (upper panel) CdSe. The symbols are results obtained using Bergstresser and Cohen (BC) empirical pseudopotential (Ref. 77), and the solid lines are the results obtained from the nonlinear fit.

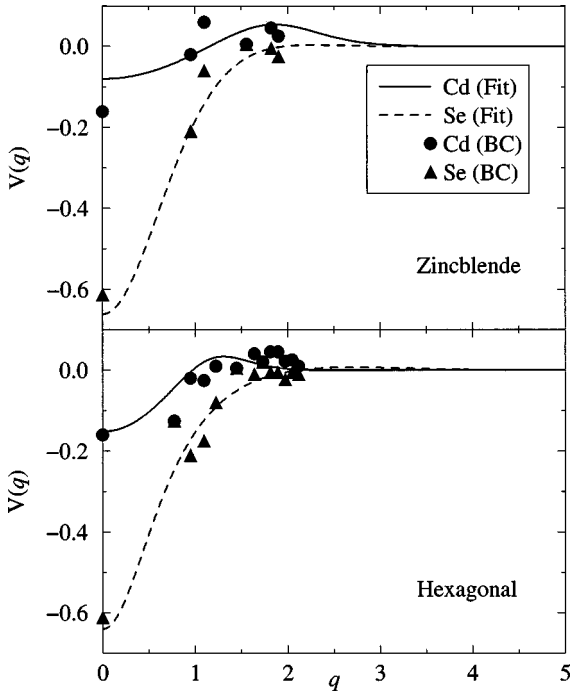

FIG. 2. The empirical pseudopotential for Cd and Se atoms plotted in momentum space. The symbols are the form factors of Bergstresser and Cohen (BC) (Ref. 77), and the solid and dashed lines are the results of the nonlinear fit to the bulk band structure. Note that the fits are not done directly to the form factors.

The other ingredient needed to complete the description of our Hamiltonian (which is not required for bulk calculations) is the surface passivation. We adopt the ''ligand potential'' model of Wang and Zunger,[54] which places a short range electrostatic potential near the surface atoms. The effective ligand potentials are taken to be Gaussians

$$V_\beta^{\text{ligand}}(|\hat{\mathbf{r}}-\mathbf{S}_\beta|)=V_\beta^0\exp(-|\mathbf{r}-\mathbf{S}_\beta|^2/\sigma_\beta^2). \tag{3}$$

The origin of the ligand potential, $\mathbf{S}_\beta$, is taken to be in the direction of the missing bonding atom, and the distance to the passivated atom equals αR_e, where α varies depending on the atom type and the number of missing bonds; R_e is the Cd–Se bulk bond length. For hexagonal and zincblende CdSe nanocrystals a surface atom may have 1, 2 or 3 missing bonds, and therefore, the same number of ligand sites, respectively. The values of V_β^0, σ_β and α are given in Table II.

B. Filter diagonalization

It is not feasible to diagonalize directly the one-electron Hamiltonian described in Eq. (1) to obtain the desired eigenvalues and eigenstates, even for relatively small nanocrystal sizes, since we use a basis set of more than 32 768 functions even for the smallest nanocrystals. However, we must keep in mind that we are not interested in all eigenvalues and eigenstates of Eq. (1), but rather in a small set of them. We, therefore, use the filter-diagonalization method of Neuhauser and co-workers,[72–76] and introduce some small modifications.

We represent the wave functions on a three dimensional grid in real space.[84–86] This real-space representation of the wave function has recently been proposed in the context of nanocrystallite semiconductors.[87] In this representation the potential energy operator is local and is simply calculated on the grid points. Since our potential is a screened empirical pseudopotential, the long and short range Coulomb anomalies are absent, and the real-space representation converges rapidly outside the nanocrystal regime. The kinetic energy operator is nonlocal in this representation, and is evaluated using the fast Fourier transform method.[88,89]

TABLE I. The values of the pseudopotential parameters defined in Eq. (2) for the hexagonal (hex) and zincblende (zb) crystals structures.

atom	a_1 (a.u.)	a_2 (a.u.)	a_3 (a.u.)	a_4 (a.u.)
Cd (hex)	0.193	0.936	0.196	1.68
Se (hex)	−0.0291	4.40	−1.20	0.318
Cd (zb)	0.0676	1.34	0.125	0.748
Se (zb)	−0.352	3.88	−3.07	0.754

TABLE II. The values of the ligand potential parameters for Cd and Se atoms taken from the work of Wang and Zunger (Ref. 54). The numbers in parentheses indicates the number of missing bonds.

atom	V_β^0 (a.u.)	σ_β (a.u.)	α
Cd (1)	0.64	1.49	0.55
Cd (2)	0.64	1.49	0.55
Cd (3)	0.64	1.49	0.55
Se (1)	−0.384	1.49	0.25
Se (2)	−0.384	1.49	0.30
Se (3)	−0.384	1.49	0.40

We start with N_i initial guess wave functions, $|\psi_i\rangle$, which contain the target energy range. In this work the initial guess for the value of the wave function on the grid points is taken from a uniform random distribution between -1 and $+1$, and the wave function is then normalized. This choice ensures that each initial guess contains contributions from *all* eigenstates. We then employ a Gaussian filter on each initial guess[75]

$$|\psi_i(E_l)\rangle = f(\hat{H})|\psi_i\rangle = \frac{1}{\sqrt{2\pi}}\int_{-\infty}^{\infty} dt\, \exp(-t^2/2\sigma_t^2) \times \exp(it(E_l-\hat{H}))|\psi_i\rangle, \quad (4)$$

so that the wave function $|\psi_i(E_l)\rangle$ is given by

$$|\psi_i(E_l)\rangle = f(\hat{H})|\psi_i\rangle = \sigma_t \exp(-\sigma_t^2(E_l-\hat{H})^2/2)|\psi_i\rangle, \quad (5)$$

and E_l is the target energy. The choice of the Gaussian filter is not unique, and other filters can be used to obtain various electronic properties. For example, one can replace $f(\hat{H})$ with the Fermi-Dirac operator $([1+\exp(\beta(\hat{H}-\mu))]^{-1})$,[90] which was recently shown to provide extremely fast convergence for the electronic density matrix.[91] Another useful choice for the filter is $f(\hat{H})=\sin((E_l-\hat{H})t)/(E_l-\hat{H})$, which may converge the results faster than the Gaussian filter.[92]

For large values of σ_t, $|\psi_i(E_l)\rangle$ approaches asymptotically the eigenstate closest to the target energy E_l.[93] The long time propagation can be avoided by using the filter-diagonalization scheme,[72–76] which benefits from the fact that the states far from the desired energy, E_l, decay rapidly even at short times. Thus, N_f states are generated from the N_i initial guess wave functions using a small value of σ_t. The number of filter states (N_f) differs from the number of initial guess function (N_i) since we employ the filter at different energies on the same initial guess (this is done to save computer time).[72–76] Note that the filtered states are not eigenstates of the Hamiltonian but are a superposition of states with energies that are inside the window. These states are used as a basis set to obtain the eigenvalues ($\mathcal{E}_n$) and eigenstates ($|\psi_n\rangle$) of the Hamiltonian in the desired energy range.

For clarity we replace the labels i and l with m, such that m runs from 1 to $i\times l$, and the filter states are labeled $|\psi_m^f\rangle$. The eigenstates, $|\psi_n\rangle$, are then given in terms of a superposition of the filtered states $|\psi_m^f\rangle$

$$|\psi_n\rangle = \sum_{m=1}^{N_f} c_{nm}|\psi_m^f\rangle, \quad (6)$$

where the expansion coefficients, c_{nm}, are obtained from the solution of the generalized eigenvalue equation in the reduced Hilbert space (note that the filtered states, $|\psi_m^f\rangle$, are not necessarily orthogonal)[75]

$$\tilde{H}\tilde{c} = \tilde{S}\tilde{c}\mathbf{E}, \quad (7)$$

where

$$H_{mm'} = \langle \psi_m^f|\hat{H}|\psi_{m'}^f\rangle \quad (8)$$

and

$$S_{mm'} = \langle \psi_m^f|\psi_{m'}^f\rangle. \quad (9)$$

A standard singular value decomposition method is used to solve the linear equation.[75,94] This procedure resembles the renormalization group method of Baer and Head-Gordon.[95]

In the original filter-diagonalization method,[72] and its most recent variation,[75] the propagator $f(\hat{H})$ is expanded in Chebyshev polynomials. A difficulty with this choice of polynomials is that the expansion coefficients are calculated numerically, and various numerical tricks are introduced to converge the results for the coefficients.[75] To avoid these difficulties we use the Newton interpolation polynomial scheme,[85,96,97] where the propagator, $f(\hat{H})$, is approximated by the interpolation polynomial

$$f(\hat{H}) \approx P_N(\hat{H}) = \sum_{j=0}^{N} a_j R_j(\hat{H}), \quad (10)$$

$$R_j(\hat{H}) = \prod_{k=0}^{j-1} (\hat{H}-h_k), \quad (11)$$

and the coefficients take the form

$$a_0 = f(h_0), \quad a_1 = \frac{f(h_1)-f(h_0)}{h_1-h_0},$$

$$a_{j>1} = \frac{f(h_j)-P_{j-1}(h_j)}{R_j(h_j)}. \quad (12)$$

In the above equations, h_k are the support points taken to be the zeros of the $N+1$ Chebyshev polynomial.[98] This choice defines the points on the interval $[-2,+2]$, and the Hamiltonian is rescaled so that its spectrum lies in the desired interval

$$\hat{H}_s = 4\frac{\hat{H}-E_{\min}}{E_{\max}-E_{\min}} - 2. \quad (13)$$

$E_{\min}$ and $E_{\max}$ are the lowest and highest eigenvalues of the Hamiltonian, respectively. The operator $\hat{H}_s$ is the one we use in the interpolation formula. The final results for the propagated wave function is

$$|\psi_m^f\rangle = \sum_{j=0}^{N-1} a_j|\phi_j\rangle, \quad (14)$$

and we use the recursion relation to generate the $|\phi_j\rangle$ ($|\phi_0\rangle = |\psi_i\rangle$)

$$|\phi_{j+1}\rangle = (\hat{H}_s - h_j)|\phi_j\rangle. \quad (15)$$

The main advantage of the filter-diagonalization method is that one can use the same initial guess for different values of E_l, and thus use the same interpolation polynomial (with different expansion coefficients) to obtain many states simultaneously. There is a balance between the propagation width (σ_t) and the number of linearly independent states one obtains from propagating a single initial guess state. This balance is related to the energy spacing and the energy range of the Hamiltonian. In this work we set the propagation width so that we obtain $\sim$20 states for each initial guess functions.

Therefore, we apply the filter to several different initial guess function to obtain all states in the desired energy range.

C. The self-consistent reaction-field method

We use the reaction field continuum model,[69–71] to study the solvation of the CdSe nanocrystal. The treatment of explicit solvent structures is left for future study. Here we develop a quantum mechanical approach which is consistent with the empirical pseudopotential method.

The nanocrystals studied in this work are taken to be spherical with a corrugated surface, and are arranged in the hexagonal crystal structure (unless otherwise noted). The reaction field continuum model requires as an input the specific shape of the boundary of the solvated particle. In this work we assume a spherical boundary with a given radius R_c,[29,68] and thus neglect the surface corrugation due to the microscopic atomic structure. Since the solution of the reaction field inside the sphere for a given charge distribution is known analytically,[99] there is no need to solve the Poisson equation.[100] The starting point of our derivation is the reaction field Hamiltonian within the Born–Oppenheimer approximation[101,102]

$$\hat{\mathcal{H}}_{\rm tot}=\sum_{\alpha=1}^{N_e}\hat{H}_\alpha-\sum_{\ell m} g_\ell\langle\Psi|\hat{M}_{\ell m}|\Psi\rangle\hat{M}_{\ell m}, \tag{16}$$

where $\hat{H}_\alpha$ is given by Eq. (1) for each electron α. The multipole moment operator for N_e electrons, and N_n nuclei is given by

$$\hat{M}_{\ell m}=\sqrt{\frac{4\pi}{2\ell+1}}\left(\sum_{\alpha=1}^{N_e}(-e)\hat{r}_\alpha^\ell Y_{\ell m}(\hat{\omega}_\alpha)+\sum_{\alpha=1}^{N_n}Q_\alpha R_\alpha^\ell Y_{\ell m}(\Omega_\alpha)\right), \tag{17}$$

where $\hat{r}_\alpha$ and $\hat{\omega}_\alpha$ are the position operators in polar coordinates for electron α, R_α, and Ω_α are the polar coordinates of atom α, $Y_{\ell m}(\Omega)$ are the spherical harmonics, and Q_α is the nuclear charge of atom α (which is taken to be the valence charge of each atom, i.e., $+2$ for Cd and $+6$ for Se). The coupling factors, g_ℓ, are given by

$$g_\ell=\frac{1}{2R_c^{2\ell+1}}\frac{(\ell+1)(\epsilon-1)}{((\ell+1)\epsilon+\ell)}, \tag{18}$$

where ϵ is the dielectric constant outside the sphere of radius R_c. In the spirit of the one-electron empirical pseudopotential method, we take the total wave function to be a product of one-electron wave functions

$$|\Psi\rangle=\prod_{\alpha=1}^{N_e}|\psi_\alpha\rangle \tag{19}$$

and we populate only two electrons in each state similar to a density functional formalism.

The many-electron Hamiltonian in Eq. (16) is separable, and after some tedious algebra is reduced to a single-electron Hamiltonian given by

$$\hat{\mathcal{H}}=\hat{H}-\sum_\ell g_\ell\hat{r}^\ell\int d\mathbf{x}\rho(\mathbf{x})x^\ell P_\ell(\cos(\gamma)), \tag{20}$$

where $P_\ell(\cos(\gamma))$ are the Legendre polynomials, γ is the angle between the position vectors $\mathbf{r}$ and $\mathbf{x}$, and the total charge density $\rho(\mathbf{x})$ is

$$\rho(\mathbf{x})=-e\sum_{\alpha=1}^{N_e}\langle\psi_\alpha|\mathbf{x}\rangle\langle\mathbf{x}|\psi_\alpha\rangle+\sum_{\alpha=1}^{N_n}Q_\alpha\delta(\mathbf{x}-\mathbf{R}_\alpha). \tag{21}$$

The pseudopotential reaction-field Hamiltonian [cf. Eq. (20)] depends on the total electronic charge, and is therefore, nonlinear. The solution is obtained by iterating the Schrödinger equation until convergence is achieved, i.e., until the total energy of two iterations agree within a specified tolerance.

III. ELECTRONIC PROPERTIES OF ISOLATED CDSE NANOCRYSTALS

A. Density of states and band gap

The first set of calculations is performed on isolated nanocrystals in order to study the dependence of the density of states and the band gap on nanocrystal size using our pseudopotential. We use a real space grid of $32\times32\times32$ for the small nanocrystals (14 Å$\leqslant d<$20 Å where d is the diameter), $48\times48\times48$ for the medium size nanocrystals (20 Å$\leqslant d<$30 Å), and $64\times64\times64$ for the large nanocrystals (30 Å$\leqslant d<$40 Å), etc. The range of the grid is larger than the nanocrystal diameter by 6–8 atomic units. For all the results reported in this section we use an Newton interpolation of length $N=2048$ unless otherwise noted. The propagation width [cf. Eq. (5)] is determined from the relation[75]

$$\sigma_t=\frac{N}{7.7(E_{\rm max}-E_{\rm min})}, \tag{22}$$

and a typical energy range is $E_{\rm max}-E_{\rm min}\approx10$ atomic units.

The density of states for each nanocrystal is obtained by applying the filter-diagonalization method described in the previous section. A set of initial random trial functions, which contained the desired energy range, is propagated using the Gaussian filter, and then used to solve the generalized eigenvalue equation [cf. Eq. (7)]. We note that our approach is closely related to the generalized moment approach, recently applied to nanocrystals,[103] however, additional work is done in order to obtain the eigenstates, which are then used for other purposes (see below). In return, the density of states is much more accurate.

In Fig. 3 we plot the density of states for a wide range of nanocrystal sizes. For clarity of presentation the lower valence band, which is characterized by the surface states of the Se atoms that have missing bonds, is not shown. There are several interesting features of the density of states which have been seen in all previous studies. As the nanocrystal size increases the gap decreases (see also Fig. 4) and the width of the upper valence band increases (the lower valence band is not shown). We also observe that the continuous tail of the density of states above the conduction band observed in bulk calculations breaks into several individual peaks due

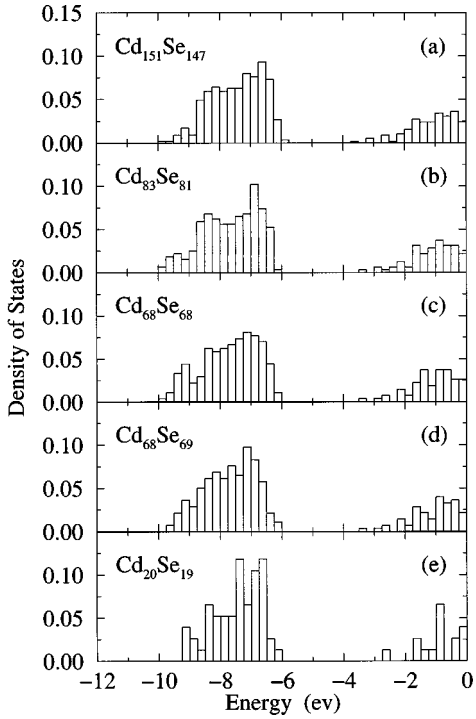

FIG. 3. The density of states for CdSe nanocrystals. The results are normalized so that the *total number* of valence states is unity.

to quantum confinement. The individual valence states form a continuum density of states only on the scale of the plot.

In panels (c) and (d) we show the density of state for two nanocrystals that are identical in size, however, one is centered around the Se atom ($Cd_{68}Se_{69}$) and the other is centered around the center of the unit cell ($Cd_{68}Se_{68}$). We refer to these two types of nanocrystals as ''Se-centered'' and ''cell-centered,'' respectively. The density of states and the band gap are very similar for these two nanocrystals, however, we find that the total number of electronic states below the gap equals the number of paired electrons only for $Cd_{68}Se_{68}$, and there is an ''excess'' state for $Cd_{68}Se_{69}$. This is also the case for other nanocrystals studied here, and in general we find missing states when $N_{Cd}>N_{Se}$, and excess states when $N_{Cd}<N_{Se}$. For $N_{Cd}\neq N_{Se}$ the total number of states below the gap (i.e., valence states) does not equal the total number of paired valence electrons.

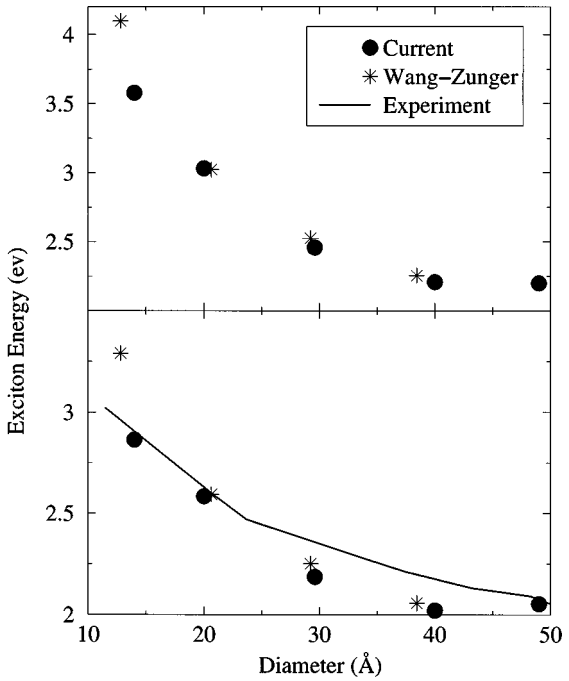

FIG. 4. Exciton energies of CdSe nanocrystals. The results of Wang and Zunger are from Ref. 54, and the experimental results are from Ref. 11. The upper panel is the bare band gap and the lower panel is the gap including the electron–hole Coulomb interaction.

The missing–excess states are artifacts of the surface passivation of the nanocrystals. The ligand potentials [cf. Eq. (3)] ''push'' the states of the Cd atoms (with missing bonds) into the conduction band, and the Se atoms (with missing bonds) into the valence band, so that the gap is free of surface states. Physically, the Cd atoms (with missing bonds) can be regarded as donors, and the Se atoms (with missing bonds) as acceptors. Since the total number of states is much larger than the number of missing–excess states (the later depends on $|N_{Cd}-N_{Se}|$) the net effect of this phenomena on the density of states is negligibly small, as can be clearly seen in Fig. 3. Because of this artifact, our present calculation does not correctly yield the states localized on the surface atoms, however, since we know exactly the number of missing–excess states, we can correctly predict the number of occupied states, and thus obtain the band gap and other electronic properties. We further discuss this point below, when we present the results for the electronic charge calculations.

The exciton energies with and without the electron–hole Coulomb energy (defined below) are shown in the lower and upper panels of Fig. 4, respectively. The results are compared to other calculations,[42,54] and to experimental results.[11,14,15,17,104] The valence band maximum (VBM) and the conduction band minimum (CBM) are obtained by filtering two states, one with a target energy slightly above the VBM ($E_m=-5.4$ eV), and the other with a target energy slightly below the CBM ($E_m=-3.8$ eV). We thus avoid the need to compute all valence states and focus on obtaining only the highest occupied molecular orbital (HOMO) and LUMO, a procedure that scales linearly with the system size.

The propagation width (σ_t) is chosen to converge the value of the gap, $E_g(d)=E_{CBM}(d)-E_{VBM}(d)$, to within a desired tolerance. Additionally, we also calculate the standard deviation, $(\delta E_\alpha)^2=\langle\psi_\alpha|(H-E_\alpha)^2|\psi_\alpha\rangle$, for each state. A typical value of the standard deviation is found to be below 10^{-8} atomic units. Due to the higher density of states near the VBM, the HOMO converges more slowly than the LUMO. We, therefore, use a larger Newton interpolation length for the HOMO, and for similar reasons increase the Newton interpolation length with the size of the nanocrystal.

We follow the procedure suggested by Wang and Zunger[54] to obtain the exciton energy, which is given by[2,3,5,105,106]

$$E_{ex}(d)=E_g(d)-\frac{3.572}{d\epsilon^{nc}(d)}. \tag{23}$$

The size dependent dielectric constant of the nanocrystal, $\epsilon^{nc}(d)$, is approximated by[54]

$$\frac{1}{\epsilon^{nc}(d)} = \frac{1}{\epsilon_{\infty}^{nc}(d)} - \beta(d)\left(\frac{1}{\epsilon_{\infty}^{nc}(d)} - \frac{1}{\epsilon_{\infty}^{nc}(d)+3.5}\right), \quad (24)$$

and the electronic contribution to the total polarizability is

$$\epsilon_{\infty}^{nc}(d) = 1 + \frac{\epsilon_{\infty}^{\text{bulk}} - 1}{1+(7.5\ \text{Å}/d)^{1.2}}. \quad (25)$$

$\beta(d)$ indicates how much the ions participate in the screening, and is interpolated from the results of Ref. 54. Readers who are interested in more details concerning the derivation of Eqs. (24) and (25) should consult the original work of Wang and Zunger.[54]

In the upper panel of Fig. 4 we compare our results for the exciton energies excluding the electron–hole Coulomb term [i.e., the bare gap energies $E_g(d)$], to the results obtained by Wang and Zunger[54] using the local density derived semiempirical pseudopotentials.[83] The agreement between the two calculations is very good, albeit the fact that the scaling with respect to the nanocrystal size is somewhat different. In the lower panel of Fig. 4 we compare our results for the exciton energies including the electron–hole Coulomb term to the experimental results of Murray *et al.*[11] who have fabricated CdSe crystallites with a remarkably narrow size dispersion ($<5\%$). Since the experimental results of other groups[14,15,17] are very close to those reported by Murray *et al.* we do not show them here for the clarity of presentation. We find good agreement between our calculations and the experimental results for most nanocrystal sizes. The calculated confinement energy $[E_{ex}(d)-E_{ex}(\infty)]$ follows approximately the law $d^{-\alpha}$, with $\alpha=1.15$, which is slightly below both the results of Wang and Zunger,[54] and the results of Albe, Jouanin, and Bertho[42] (who recently developed a tight-binding model for CdSe nanocrystals), but is closer to the experimental value.

We conclude that our local empirical pseudopotential provides realistic description for the density of states and the band gap, and therefore, is adequate to use for other electronic properties reported below.

B. Electronic charge density

The electronic charge density, $\rho_e(\mathbf{r})$, is given in terms of the eigenstates of the Hamiltonian [Eq. (1)]

$$\rho_e(\mathbf{r}) = -e\sum_{\alpha=1}^{N_e} \langle\psi_\alpha|\mathbf{r}\rangle\langle\mathbf{r}|\psi_\alpha\rangle, \quad (26)$$

where the sum runs over all occupied states. To ensure that the nanocrystal is neutral we normalize the electronic charge density, so that the total electronic charge equals the total nuclear charge (in the present calculations we describe only the valence charge, i.e., 2 Cd electrons and 6 Se electrons). This is required due to the problem mentioned in the previous subsection concerning the missing–excess states. Since the number of missing–excess states is relatively small compared to the total number of occupied states, their effect on the electronic charge density should be negligibly small.

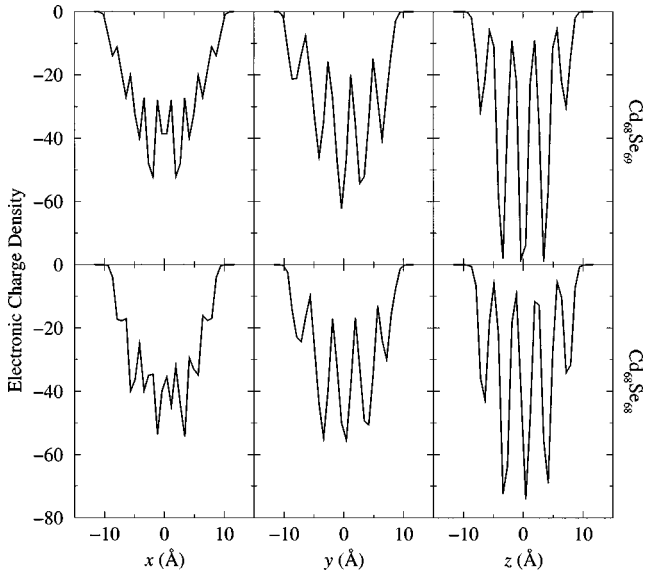

FIG. 5. Integrated electronic charge density of CdSe nanocrystals. The charge density is normalized such that the integral in each direction equals the total electronic charge. Note the differences between the two nanocrystals along the x and y directions.

We note in passing that the electronic charge density can be obtained from the trace over the electronic density matrix, which can be approximated by the Chebyshev (or Newton) expansion of the Fermi-Dirac density matrix.[90,91] For the present problem we find that our implementation of the filter-diagonalization method is more efficient than the one-step renormalization group method recently introduced by Baer and Head-Gordon,[95] since we obtain several states simultaneously using the same Newton interpolation polynomial.

The integrated electronic charge density along the [100] (x axis), [010] (y axis), and [001] (z axis which is the c axis of the hexagonal lattice), is shown in Figs. 5 and 6. The

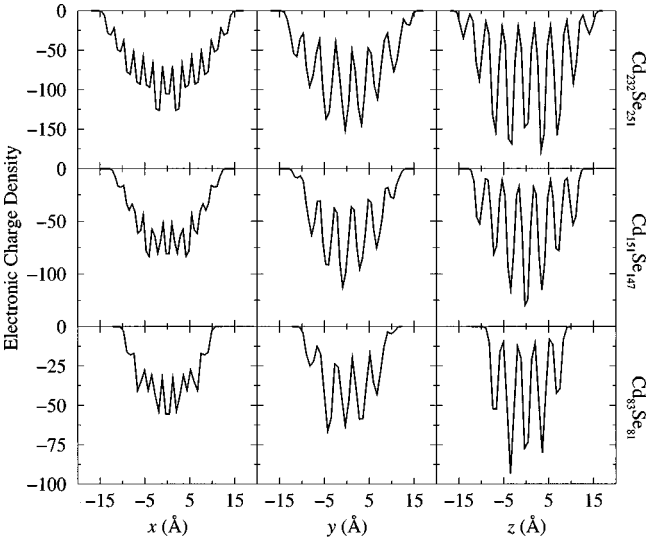

FIG. 6. Integrated electronic charge density of CdSe nanocrystals. The charge density is normalized such that the integral in each direction equals the total electronic charge. The diameter is 21.2, 25, and 29.6 Å for $Cd_{83}Se_{81}$, $Cd_{151}Se_{147}$, and $Cd_{232}Se_{251}$, respectively.

TABLE III. The dipole moment of CdSe nanocrystals along the *x*, *y*, and *z* directions, and its magnitude.

	μ_x (a.u.)	μ_y (a.u.)	μ_z (a.u.)	$\lvert\mu\rvert$ (a.u.)
$Cd_{20}Se_{19}$	0.0	0.6	−67.4	67.4
$Cd_{41}Se_{39}$	0.0	0.5	23.2	23.2
$Cd_{68}Se_{69}$	0.0	1.2	14.2	14.3
$Cd_{83}Se_{81}$	0.0	−0.2	−153.6	153.6
$Cd_{151}Se_{147}$	0.0	0.1	59.4	59.4
$Cd_{232}Se_{251}$	0.0	−4.4	−28.1	28.4

TABLE IV. The diagonal elements of the second moment of the charge density for CdSe nanocrystals. The off-diagonal elements are typically smaller by more than two orders of magnitude and, therefore, are not given in the table. $|Q|$ is the average magnitude of the diagonal elements of the second moment.

	Q_{xx} (a.u.)	Q_{yy} (a.u.)	Q_{zz} (a.u.)	$\lvert Q\rvert$ (a.u.)
$Cd_{20}Se_{19}$	−110.5	−114.5	−23.4	82.8
$Cd_{41}Se_{39}$	−597.7	−578.9	595.0	590.5
$Cd_{68}Se_{69}$	−671.0	−655.7	−0.5	442.4
$Cd_{83}Se_{81}$	−540.2	−633.7	−430.9	535.0
$Cd_{151}Se_{147}$	583.4	779.7	−2184.0	1182.3
$Cd_{232}Se_{251}$	−3226.5	−3283.2	−3986.3	3498.7

general features common to all nanocrystals are that the electronic charge is centered around the Se atoms consistent with predictions of density functional calculation for bulk CdSe[107] and with high resolution electron microscopy results,[18] and that the electronic charge drops rapidly outside the nanocrystal range.

In Fig. 5 we compare the integrated electronic charge density for nanocrystals that are identical in size, however one is Se-centered ($Cd_{68}Se_{69}$) and the other is cell-centered ($Cd_{68}Se_{68}$). Even though the two nanocrystals are very similar in size, their electronic properties are somewhat different. The $Cd_{68}Se_{69}$ nanocrystal belongs to the C_{3v} group symmetry, which is found to be the group symmetry of highly annealed hexagonal CdSe nanocrystals.[18] The top and bottom surfaces along the *z* direction are Cd and Se terminated, respectively. The electronic charge density reflects mainly the symmetry of the Se atoms, so that along both the *x* and *z* directions the electronic charge density is symmetric around the center (the *x* direction is chosen to lie in one of the σ_v planes of reflection). The $Cd_{68}Se_{68}$ is cell centered, and therefore, belongs to a lower symmetry group. The major differences between the two charge densities are in the $x-y$ plane. We note that for both nanocrystals we remove surface atoms with only one remaining bond.

In Fig. 6 we plot the integrated electronic charge density of three nanocrystals ranging from $d \approx 20$ Å to $d \approx 30$ Å; all three nanocrystals are Se-centered, and belong to C_{3v} group symmetry. They differ with respect to the details of the reconstruction of the surface geometries. The top surface along the *z* direction is Cd terminated for $Cd_{83}Se_{81}$ and $Cd_{151}Se_{147}$, and is Se terminated for $Cd_{232}Se_{251}$. The bottom surface along the *z* direction is Se terminated for all three nanocrystals. Similar to the case of the smaller nanocrystal ($Cd_{68}Se_{69}$), the electronic charge density along the *x* and *z* directions is symmetric around the center.

C. Multipole moments

Given the electronic charge density, we calculate the dipole and higher multipole moments of several nanocrystals. Our calculations are based only on the valence electronic and nuclear charge densities, within the empirical pseudopotential framework. The origin of the multipole expansion is taken to be the center of the total (electronic+nuclear) charge densities, which happens to fall near the centered Se atom. The results for CdSe nanocrystals that are Se-centered are summarized in Tables III and IV.

The dipole moments in the $x-y$ plane are very small for nanocrystals that are Se-centered. This is not the case for cell-centered nanocrystals which can have finite dipole moments in the $x-y$ plane. Both $Cd_{68}Se_{69}$ and $Cd_{232}Se_{251}$ have dipole moments that are comparable to the screened experimental values of Guyot-Sionnest and co-workers,[25,26] while $Cd_{83}Se_{81}$ has the largest (among the structures studied here) dipole moment along the *z* direction. In general, we do not find any systematic behavior of the dipole moment as we vary the nanocrystal size. The dipole moment strongly depends on the detailed structure of the nanocrystal, and may vary significantly upon small structural changes. We also find that there are no correlations between the surface termination and the direction or magnitude of the dipole moment. We also carried out calculations for a zincblende crystal structure, and found vanishing dipole moments in all three directions.

The large value of the dipole moment can result from the lack of inversion symmetry in hexagonal nanocrystals,[108] or from charge localized on the surface (surface states). Our results support the classical model of Huong and Birman[108] who argue that the spontaneous polarization and large dipole moments in nanocrystals is due to lack of inversion symmetry in hexagonal nanocrystals. A close examination of the structure of $Cd_{83}Se_{81}$ reveals the fact that it is highly symmetric along the *z* direction (it has a plane of symmetry for Cd atoms and for Se atoms separately) so that the dipole of each unit cell of the hexagonal crystal structure adds up to give a large value for the dipole moment (the same is true for $Cd_{20}Se_{19}$). This is not the case for the other two nanocrystals ($Cd_{68}Se_{69}$ and $Cd_{232}Se_{251}$), and it appears that there are some structural cancellations that decrease the dipole moment along the *z* direction. We also modified the ligand potential used to model the passivation of the surface atoms and found that the dipole moment is almost insensitive to the value of the potential at the surface. This strongly suggests that the dipole moment is a structural property of hexagonal CdSe nanocrystals and not due to the presence of an electron localized on the surface.

Regarding the second moment of the charge density (the quadrupole is given in terms of the elements of the second moment), the diagonal elements seem to follow a more systematic trend with increasing nanocrystal size, i.e., the second moment of the charge density increases with size. The off-diagonal elements are smaller by at least two orders of

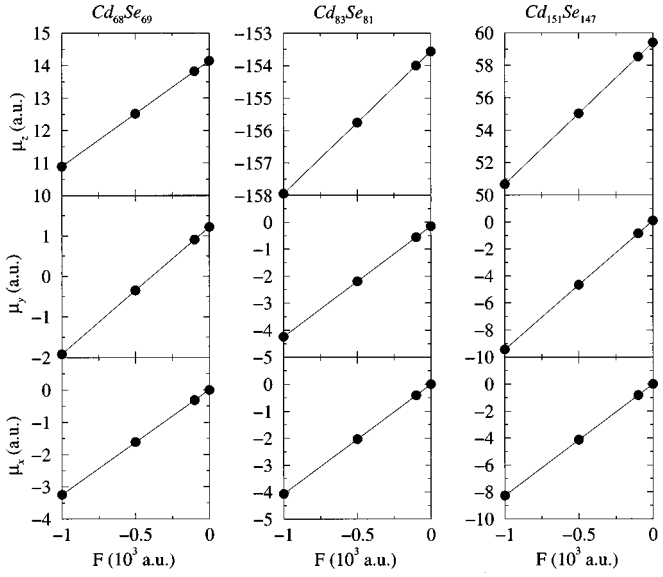

FIG. 7. Plots of the dipole moment as a function of the applied external field. The direction of the field in each calculation is taken along the direction of the observed dipole moment. The response of the system is linear for fields smaller than 10^{-3} atomic units.

magnitude (except for the case of $Cd_{68}Se_{69}$ which has a vanishing Q_{zz} term), and therefore, are not given in the table. The values of the second moment of the charge density along the different directions are similar in most cases, reflecting the spherical shape of the nanocrystals. Nevertheless, these particles are highly anisotropic due to the large dipole moment along the *c* axis.

D. Electronic polarizabilities

The electronic polarizabilities of the CdSe nanocrystals are calculated using a finite-field method.[109–111] We add an external electrical field into the Hamiltonian by adding one term to the effective empirical potential

$$\hat{H}_F = \hat{H} - e\mathbf{F}\cdot\mathbf{r}, \tag{27}$$

where $\hat{H}$ is the empirical pseudopotential Hamiltonian given by Eq. (1), and $\mathbf{F}$ is the applied electric field. The polarizability is defined by

$$\alpha_{ij} = \frac{\partial \mu_i}{\partial F_j}, \quad i,j = \{x,y,z\}, \tag{28}$$

where μ_i are the dipole moments along the $i=\{x,y,z\}$ axes.

The different elements of the polarizability tensor are obtained by applying a finite field in the *x*, *y*, and *z* directions. In Fig. 7 we plot the value of the dipole moment as a function of the applied external field for three nanocrystals. It is clear that the results are well inside the linear response regime, and that the direction of the induced dipole is in the direction of the applied external field. We must point out that we did not relax the ionic positions in the finite field calculations, and thus obtain only the electronic polarizability. Unlike the results for Si and GaAs,[111] which indicate that the ionic relaxation affects the calculated polarizabilities only within 2% to 3%, we expect that the ionic polarizability of CdSe will definitely contribute to the total polarizability.

TABLE V. The diagonal elements of the electronic polarizability tensor (in units of $Å^3$/atom) obtained from the finite field method. The result for the bulk is obtained from the Clausius–Mossotti relation using $\epsilon_\infty^{\text{bulk}} = 6.2$.

	α_{xx}	α_{yy}	α_{zz}	$\langle\alpha\rangle$
$Cd_{68}Se_{69}$	3.504	3.396	3.528	3.476
$Cd_{83}Se_{81}$	3.678	3.692	3.963	3.778
$Cd_{151}Se_{147}$	4.197	4.754	4.347	4.433
bulk				4.25

The diagonal elements of the polarizability tensor are then calculated from the slopes of a linear fit to the results shown in the Fig. 7. The values are summarized in Table V, along with the averaged polarizability, $\langle\alpha\rangle = \frac{1}{3}(\alpha_{xx}+\alpha_{yy}+\alpha_{zz})$, which is the property measured in experiments. We also include the electronic polarizability of the bulk estimated from the Clausius–Mossotti relation, using $\epsilon_\infty^{\text{bulk}} = 6.2$. Surprisingly, the polarizabilities are very similar along the three direction, and it seems that the large dipole along the *c* axis does not influence the polarizability along this direction (this reflects the spherical shape of the nanocrystals). The electronic polarizability per atom slightly increases with increasing nanocrystal size concomitant by the decrease in the energy gap. Our results are consistent with those of Wang and Zunger[54] for the dielectric constant of CdSe nanocrystals (for $Cd_{83}Se_{81}$, which is a nanocrystal common to both studies, we obtain a dielectric constant of 4.86 using the Clausius–Mossotti relation, which is in excellent agreement with the direct calculation of Wang and Zunger). Hence, the total electronic polarizability increases approximately with the volume of the nanocrystal. The off diagonal elements of the polarizability tensor are typically smaller by at least two orders of magnitude than the diagonal elements, and therefore, are not given in the table.

E. Long range electrostatic and dispersion interactions

An interesting spinoff of the current results is directly related to the long range interactions between two nanocrystals. Since hexagonal CdSe nanocrystal may have a large dipole moment, it is possible that the dominant interaction term between two CdSe nanocrystals is given by the electrostatic interaction and not by the dispersion interaction expected for large particles.[112] Indeed we find that for neutral CdSe nanocrystals with hexagonal crystal structure the dipole–dipole electrostatic interaction term, which depends on R^{-3} (where *R* is the distance between the centers of the two nanocrystals) is the dominant interaction term at large interparticle separations (≈ 5 times the size of the particles) for all nanocrystals studied in this work. It is by far larger than the dispersion interactions (van der Waals interactions), which scale as R^{-6} and depend on the total polarizability of the nanocrystals at large separations. We also find that at separations which are on the order of the nanocrystal size the dipole–quadrupole (R^{-4}), and dipole–octupole, and quadrupole–quadrupole (R^{-5}) interaction terms are compa-

rable in size to the dipole-dipole interaction term. This situation in which the electrostatic interactions are stronger than the dispersion interactions is very similar to the case of water which also has a large dipole moment. Hence, the interactions between hexagonal CdSe nanocrystals are typical of molecular type interaction and not of the Hamaker[112] (dispersion) interactions expected for large particles.

Our current picture is only valid for large separations between the nanocrystals compared to the size of the particles. However, understanding various collective properties, such as the self-assembly of nanocrystals[113,114] or the formation of crystals of nanoparticles,[115] requires a more rigorous study of the interactions between nearby (or almost touching) nanocrystals. At this point it is still an open question whether the electrostatic will dominate over the dispersion also at short separations.

IV. THE EFFECT OF THE SURROUNDINGS

We study the effects of the surroundings on various electronic properties of CdSe nanocrystals using the reaction field continuum model.[69,70] We diagonalize the one electron pseudopotential reaction field Hamiltonian [Eq. (20)] iteratively using the eigenstates of the isolated nanocrystal, until the convergence of the eigenvalues is within 10^{-4} of their initial values. This requires at most 3 to 4 iterations. For nanocrystals with diameter above 20 Å we carried out only three iterations that converge the eigenvalues to within 10^{-3} of their initial value. The use of the isolated eigenstates as a basis set to study the effects of the surroundings is advantageous for the size of nanocrystals studied in this work, since the direct diagonalization of the Hamiltonian within this subspace is faster than performing the filter-diagonalization step in each iteration. However, since this procedure scales with the cube of the number of basis functions, for larger nanocrystals a direct filter-diagonalization procedure at each iteration will be faster. The number of Legendre polynomials used in the one-electron pseudopotential reaction field Hamiltonian [Eq. (20)], depends on the particular grid point ($\mathbf{r}$), and is chosen to converge the value of the potential at that given grid point to within 10^{-8} of its initial value. For grid points near the edge of the sphere we use more than 5000 Legendre polynomials, however a more typical value is below 50.

A. Collective state properties

The changes in the total electronic charge density are very small with increasing dielectric constant ϵ, and cannot be seen on the scale of Figs. 5 and 6. The individual states do mix, however, and as expected, the largest effect on the energy shifts are obtained for states that are near the surface. We did not find any states well inside the band gap, but some surface states do appear near the valence band maximum. These surface states may leak into the gap, depending on the magnitude of the dielectric constant outside the nanocrystal, and on the magnitude of the interaction between the nanocrystal and its surroundings. We believe that the appearance of these surface states depends strongly on the details of the surface passivation, and for other passivation potentials the

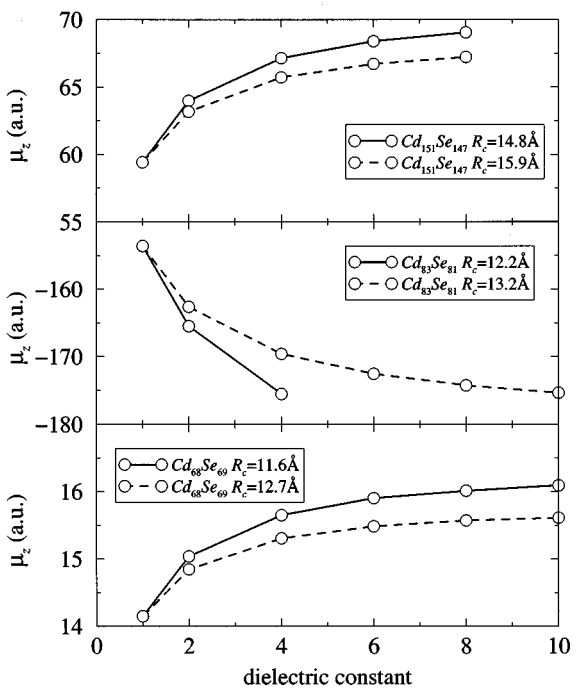

FIG. 8. Plots of the dipole moments along the z direction vs the dielectric constant outside the nanocrystal for two values of the cutoff radii.

nature of these states may change. We return to this point below when we discuss the absorption spectrum.

In Figs. 8 and 9 we show the dependence of the first and second moments of the charge density on the dielectric constant (ϵ) outside the nanocrystal sphere for two different cutoff radii (R_c). The results are shown for three nanocrystals that are Se-centered, and thus have dipole moments only along the z direction. These values are chosen to cover the range of dipoles from relatively small values ($Cd_{68}Se_{69}$) to large values ($Cd_{83}Se_{81}$), and a range of sizes. We use cutoff radii in the reaction field calculations which are larger than the nanocrystal radii to incorporate the effect of the ligand

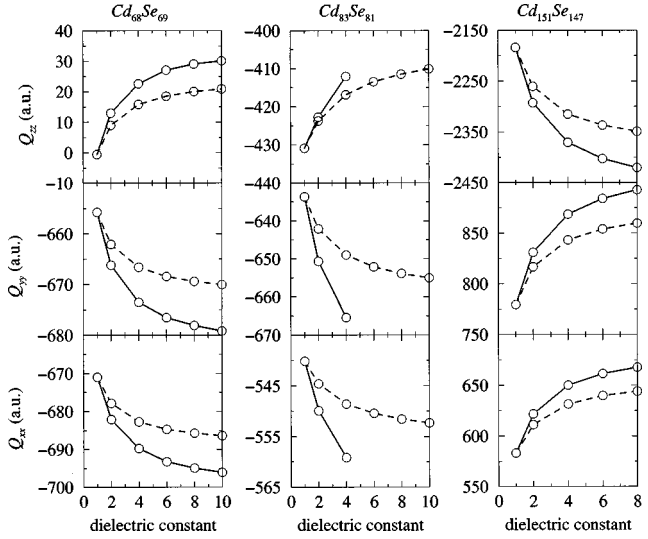

FIG. 9. Plots of the diagonal elements of the second moment of the charge density vs the dielectric constant outside the nanocrystal for two values of the cutoff radii.

passivation layer. Since the exact passivation width is unknown, we study the solvation as a function of this width by changing the cutoff radius (R_c).

Even though the change in the electronic charge density is extremely small ($\approx 1\%-3\%$), we observe a change of up to 15% in the dipole moments (Fig. 8). The absolute value of the dipole moment increases with increasing dielectric constant for all the nanocrystals studied here. The relatively large change in the dipole moment is directly related to the large size of the nanocrystals. The dipole moment is given by $\boldsymbol{\mu}=\int d\mathbf{x}\rho(\mathbf{x})\mathbf{x}$, where $\rho(\mathbf{x})$ is the total charge density [cf. Eq. (21)]. The small changes in the electronic charge density are amplified in the dipole calculations due to the large values of $\mathbf{x}$. Moreover, these nanocrystals have a large surface area, and thus even very small changes in the charge at the surface give rise to fairly large changes in the dipole moment. Similar arguments also apply in explaining the behavior of the second moment of the charge density shown in Fig. 9.

The effect of the width of the passivation layer on the first and second moments of the charge density is also evident in Figs. 8 and 9. For simplicity we assume that the dielectric constant in the passivation layer is $\epsilon=1$. This implies that the change in the passivation layer is modeled by a change in the cutoff radius used in the reaction field calculations. The smaller the width of the passivation layer, the larger is the interaction of the nanocrystals with its surroundings, and hence the larger are the changes in the multipole moments.

Despite the large dipole moments of hexagonal CdSe nanocrystals, the total ground state is not very polarizable (for comparison, the dipole moments of water changes from 1.85 D in the gas phase to 2.5 D in liquid phase). In general we find two major effects that influence the change in the multipole moments with the dielectric constant outside the nanocrystal — the variation in the nanocrystal size and the magnitude of its multipoles. The variation in size gives rise to variations in the surface area. Large nanocrystals have large surface area, and thus larger contributions to the changes in the multipole moments due to changes in the surface charge. The other effect is related to the interaction potential between the nanocrystal and its surroundings which is directly proportional to the multipole moments [cf. Eq. (16)]. Hence, nanocrystals with larger multipoles will have larger changes in the electronic charge density, and thus larger changes in the multipole moments as one varies ϵ.

B. Single state properties

So far we have discussed the solvation effects on the total ground state electronic properties, and also described qualitatively the effects of the surroundings on single valence states which are localized near the surface. In this subsection we focus on single excited states, such as the LUMO, which can be much more polarizable, and the results shown in this subsection support this prediction.

In Fig. 10 we plot the energy shifts $[\Delta E=E_{\mathrm{LUMO}}(\epsilon)-E_{\mathrm{LUMO}}(\epsilon=1)]$ of the LUMO as a function of the dielectric constant outside the nanocrystal. The magnitude of the energy shifts increases with increasing dielectric constant for all four nanocrystals shown in the figure. We also calculate

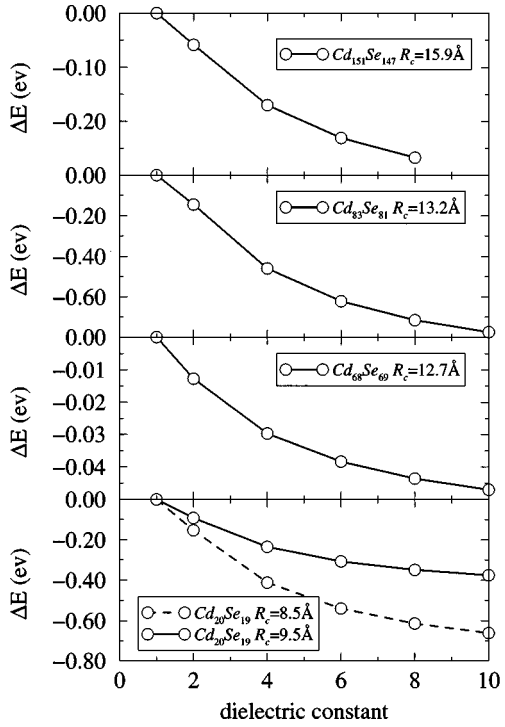

FIG. 10. Plots of the energy shifts, $\Delta E=E_{ex}(\epsilon)-E_{ex}(\epsilon=1)$, vs the dielectric constant outside the nanocrystal. Note the small shifts for $Cd_{68}Se_{69}$ and the large shifts for $Cd_{83}Se_{81}$.

the average energy shifts for the valence states, which are different from the energy shifts observed for the LUMO state. Therefore, we can conclude that the energy shifts of the LUMO are a combination of the solvation of the nanocrystal and the changes observed in the single electronic LUMO wave function.

The smallest energy shifts are observed for $Cd_{68}Se_{69}$, due to the relatively small dipole moment of this nanocrystal. On the other hand, we find large energy shifts (≈ 1 eV) for $Cd_{83}Se_{81}$ which has the largest dipole moment among the nanocrystals studied here. The screening effect of the passivation layer is also evident in the lower panel of Fig. 10, where we plot the energy shifts of $Cd_{20}Se_{19}$ for two different values of the cutoff radius. The screening due to the passivation layer increases with increasing cutoff radius resulting in a decrease in the energy shift. We note that the energy shifts observed for the LUMO are comparable in size to the quantum confinement effect.

An even more dramatic effect occurs for the integrated LUMO probability along the z direction, which is shown in Fig. 11 for the three larger nanocrystals. The unperturbed LUMO is delocalized over the nanocrystal. The changes in the integrated LUMO probability along the z direction are relatively small for $Cd_{68}Se_{69}$. However, we find that the LUMO of $Cd_{83}Se_{81}$ has a tendency to localize on the surface, on the side opposite to the direction of the dipole moment. This occurs only for large enough dielectric constants, and for $\epsilon=2$ the LUMO is still a very delocalized state. We note that similar qualitative effects have been observed for semiconductor quantum dots within the effective mass approximation.[31] However, there are quantitative differences

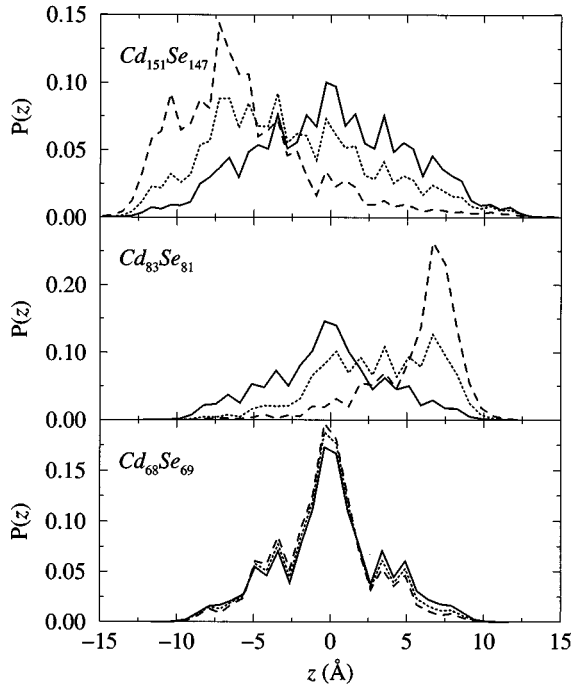

FIG. 11. Plots of the normalized integrated probability of the LUMO along the z axis. The solid, dotted, and dashed lines are for $\epsilon=1$, $\epsilon=2$, and $\epsilon=8$, respectively. The cutoff radii used in the reaction field calculations are 12.7, 13.2, and 15.9 Å for increasing nanocrystal size. Note the localization of the integrated probability for $Cd_{83}Se_{81}$ and for $Cd_{151}Se_{147}$ when $\epsilon=8$.

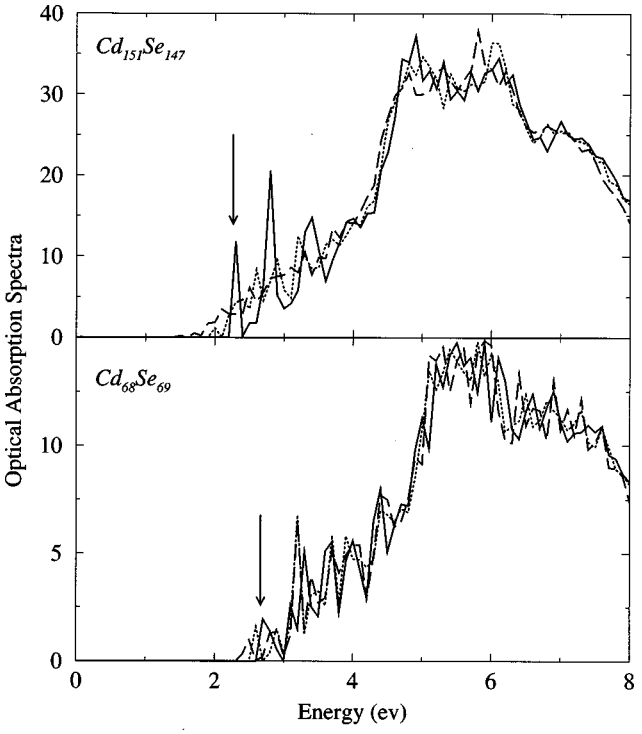

FIG. 12. Plots of the optical absorption spectra (in arbitrary units). The solid, dotted, and dashed lines are for $\epsilon=1$, $\epsilon=2$, and $\epsilon=8$, respectively. The cutoff radii used in the reaction field calculations are 12.7 Å for $Cd_{68}Se_{69}$ and 15.9 Å for $Cd_{151}Se_{147}$. The vertical arrow marks the position of the bare band gap. Note the appearance of states inside the gap as the dielectric constant outside the nanocrystals is increased.

between our molecular model and the predictions made based on the effective mass approximation, mainly with respect to the extension of the LUMO outside the nanocrystal radius, and with respect to the direction in which the LUMO moves.

We also examine the effects of the surroundings on the properties of an excess electron in CdSe nanocrystals. For simplicity we assume that the excess electron occupies the LUMO state, and we carry out similar calculations for the resultant charged nanocrystal. These calculations differ from those of the neutral system in that the total charge density entering the reaction field Hamiltonian includes a contribution from a single electron in the LUMO. Although the results for the charged system are essentially the same as those for the neutral system, the effects of the surroundings are somewhat more pronounced. We find that the multipole moments of the charged system are somewhat larger than those of the neutral system. This leads to slightly larger localization of the excess electron on one side of the nanocrystal. Furthermore, the energy shifts of the excess electronic state are larger than those of the LUMO state, due to the solvation effect of the extra charge. We do not show the results for the excess charge here since they are qualitatively the same as those for the neutral system.

C. Absorption spectrum

The absorption spectrum of the nanocrystal is proportional to the imaginary part of the dielectric constant and is given in terms of the dipole transition matrix elements (M_{fi})

$$I(E)\propto\sum_{fi}\frac{|M_{fi}^2|}{E_{fi}^2}\delta(E-E_{fi}), \tag{29}$$

where $E_{fi}=E_f-E_i$ is the transition energy, the dipole transition matrix elements take the form $M_{fi}=\langle f|\hat{\mathbf{p}}|i\rangle$, and $\hat{\mathbf{p}}$ is the momentum operator. In the above equation f and i denote final and initial states, respectively.

In Fig. 12 we show the absorption spectra of $Cd_{68}Se_{69}$ and $Cd_{151}Se_{147}$ for three values of the dielectric constant outside the nanocrystals. The dominant feature of the absorption spectrum in the absence of a dielectric medium outside the nanocrystal is the presence of a few absorption peaks near the band gap energy (solid line in both panels) characteristic of molecular spectra. These peaks were also observed in previous studies,[11,54] and are absent from nanocrystals made from indirect-gap materials such as Si.[52]

There are two main features that are due to the interaction between the nanocrystal and the environment. The first is related to the broadening and overlap of these individual peaks. As the dielectric constant outside the nanocrystal increases the overlap between the peaks increases until the peaks disappear. This broadening is not associated with the lifetime of the states, but its origin is in changes observed for the oscillator strength due to the coupling to the surroundings. The other feature is the appearance of states inside the band gap. These are not ''pure'' surface states, however, they are localized near the surface along the preferred z direction, and thus are referred to as ''quasi surface states.''

Since the LUMO is also localized along the *z* direction, the overlap of these quasi surface states with the LUMO is stronger and can be detected by absorption spectroscopy. The presence of surface states in the gap depends strongly on the passivation of the surface and on the interactions with the environment as clearly can be seen in the figure. We note that surface states have been reported for CdSe quantum films[116] and for CdSe nanocrystals[117] using conductance spectroscopy and other complementary methods.[118] The appearance of surface states inside the gap for CdSe nanocrystals was shown to strongly depend on the wetting of the surface.[119]

V. CONCLUDING REMARKS

We have carried out a detailed study of the electronic properties of CdSe nanocrystals in the absence and presence of a dielectric medium outside the nanocrystal. Our calculations were based on the empirical pseudopotential method, which was modified to describe the finite nanocrystal system. We developed a self-consistent reaction field method to be used with the empirical pseudopotential Hamiltonian. To reduce the computational cost of the calculations, we have restricted our pseudopotential to be a local one, such that the corresponding Hamiltonian has a relatively small energy range.

The solution of the one-electron effective pseudopotential Hamiltonian was made possible by the implementation of the filter-diagonalization method (as far as we know this is the first electronic structure study using this method). We have modified the method by using a Newton interpolation polynomial instead of the Chebyshev polynomial for the filter operator, and as a results of this change, the method has become more flexible in terms of changing the filter function. Of course, the Newton interpolation polynomial has other advantages such as treating non-Hermitian Hamiltonians, in which case the interpolation points have to be chosen to reside in the complex plane.[120] The filter-diagonalization method was shown to provide an excellent framework to carry out the electronic structure calculation, in particular if one is interested in a narrow set of eigenstates, such as the HOMO and the LUMO which specify the band gap.

The first set of calculations was performed on isolated CdSe nanocrystals. The electronic properties of the nanocrystals were characterized in terms of the charge density, the multipole moments and the electronic polarizability. The valence electronic charge was found to be mainly localized near the Se atoms in agreement with predictions of density functional calculations on bulk CdSe. We find very large dipole moments for hexagonal CdSe nanocrystals along the *c* axis, which strongly depend on the exact structure of the nanocrystal and may vary significantly upon small structural changes. We have shown that the large dipole moment is present due to the lack of inversion symmetry and not due to the presence of a surface charge. For some structures we obtained rough agreement with the experimental screened values of the dipole moment measured by Guyot-Sionnest and co-workers.[25,26] The second moments of the charge density as well as the polarizabilities seem to follow a more systematic trend with changing nanocrystal size. In the context of long range interactions between nanocrystals, our results provide, for the first time, a quantitative description for the electrostatic and dispersion interactions between CdSe nanocrystals, which are important in understanding collective properties of CdSe nanocrystals. An important conclusion is that for hexagonal CdSe nanocrystals the multipole interactions are more important than the dispersion interactions for large interparticle separation.

We next developed a self-consistent reaction field method and applied it to study the effects of the surrounding on collective and single state properties of CdSe nanocrystals. The interaction of the nanocrystals with the dielectric environment increases with the magnitude of its multipole moments, and in particular the dipole moment. The valence electronic charge density depends weakly on the dielectric constant outside the nanocrystal, however, due to the large size of the particles, the multipole moments vary in a more pronounced way. Single state such as the LUMO tends to strongly localize at the surface of the nanocrystal opposite to the direction of the dipole moment when the nanocrystals were embedded in a moderate dielectric medium. We found that there is a correlation between the size of the dipole moments and the localization effect, i.e., for nanocrystals with small dipole moments, the LUMO remained delocalized over the hole nanocrystal range. Similar effects were observed for an excess electron which was assumed to occupy the LUMO of the neutral system. We have also showed the effects of the dielectric medium on the absorption spectra. The individual absorption peaks near the band gap were broadened by the dielectric medium, and quasi surface states that can be detected by absorption spectra appear inside the band gap.

This work presents a first attempt to study the effects of a surrounding polar environment on electronic properties of CdSe nanocrystals using a detailed molecular model for the nanocrystal. Our results indicate the importance of including the surroundings in the study of hexagonal CdSe nanocrystals, which have a finite dipole moment along the *c* axis. They also imply that other nanocrystals (such as GaP, CdS, and Si) with crystal structures that belong to a higher symmetry point group will not interact strongly with their environment. Further work along the directions presented in this work is currently in progress.

ACKNOWLEDGMENTS

We would like to thank Professor M. L. Cohen and Professor D. Neuhauser, Dr. R. Baer, Dr. D. R. Hamann, Dr. J. D. Gezelter, and Dr. L. W. Wang for several suggestions and discussions. E.R. acknowledges the Rothschild and Fulbright foundations for financial support. This work was supported by a grant to B.J.B. from the National Science Foundation, and by a grant to L.E.B. from the U.S. Department of Energy (Grant No. DE-FG02-98ER14861).

[1] A. Henglein, Chem. Rev. **89**, 1861 (1989).
[2] L. E. Brus, Acc. Chem. Res. **23**, 183 (1990).
[3] M. G. Bawendi, M. L. Stiegerwald, and L. E. Brus, Annu. Rev. Phys. Chem. **41**, 477 (1990).
[4] L. E. Brus, Curr. Opin. Colloid Interface Sci. **1**, 197 (1996).
[5] D. J. Norris, M. G. Bawendi, and L. E. Brus, in *Molecular Electronics: A*

'Chemistry for the 21st Century' Monograph, edited by J. Jortner and M. A. Ratner (Blackwell Science, London, 1997).
[6] S. H. Tolbert and P. A. Alivisatos, Annu. Rev. Phys. Chem. **46**, 595 (1995).
[7] A. P. Alivisatos, Science **271**, 933 (1996).
[8] A. P. Alivisatos, J. Phys. Chem. **100**, 13 226 (1996).
[9] A. Ekimov, J. Lumin. **70**, 1 (1996).
[10] M. L. Steigerwald and L. E. Brus, Annu. Rev. Mater. Sci. **19**, 471 (1989).
[11] C. B. Murray, D. J. Norris, and M. G. Bawendi, J. Am. Chem. Soc. **115**, 8706 (1993).
[12] A. A. Guzelian, U. Banin, A. V. Kadavanich, X. Peng, and A. P. Alivisatos, Appl. Phys. Lett. **69**, 1432 (1996).
[13] A. J. Nozik and O. I. Mícíc, MRS Bull. **23**, 24 (1998).
[14] M. G. Bawendi, W. L. Wilson, L. Rothberg, P. J. Carroll, T. M. Jedju, M. L. Steigerwald, and L. E. Brus, Phys. Rev. Lett. **65**, 1623 (1990).
[15] M. G. Bawendi, P. J. Carroll, W. L. Wilson, and L. E. Brus, J. Chem. Phys. **96**, 946 (1992).
[16] V. L. Colvin and A. P. Alivisatos, J. Chem. Phys. **97**, 730 (1992).
[17] W. Hoheisel, V. L. Colvin, C. S. Johnson, and A. P. Alivisatos, J. Chem. Phys. **101**, 8455 (1994).
[18] J. J. Shiang, A. V. Kadavanich, R. K. Grubbs, and P. A. Alivisatos, J. Phys. Chem. **99**, 17 417 (1995).
[19] N. C. Greenham, X. G. Peng, and A. P. Alivisatos, Phys. Rev. B **54**, 17 628 (1996).
[20] M. Danek, K. F. Jensen, C. B. Murray, and M. G. Bawendi, Chem. Mater. **8**, 173 (1996).
[21] D. J. Norris and M. G. Bawendi, Phys. Rev. B **53**, 16 338 (1996).
[22] D. J. Norris, Al. L. Efros, M. Rosen, and M. G. Bawendi, Phys. Rev. B **53**, 16 347 (1996).
[23] Al. L. Efros, M. Rosen, M. Kuno, M. Nirmal, D. J. Norris, and M. Bawendi, Phys. Rev. B **54**, 4843 (1996).
[24] M. Kuno, M. Nirmal, M. G. Bawendi, Al. L. Efros, and M. Rosen, J. Chem. Phys. **108**, 4242 (1998).
[25] S. A. Blanton, R. L. Leheny, M. A. Hines, and P. Guyot-Sionnest, Phys. Rev. Lett. **79**, 865 (1997).
[26] M. E. Schmidt, S. A. Blanton, M. A. Hines, and P. Guyot-Sionnest, J. Chem. Phys. **106**, 5254 (1997).
[27] See K. Eichkorn and R. Ahlrichs, Chem. Phys. Lett. **288**, 235 (1998) and S. Öğüt, J. R. Chelikowsky, and S. G. Louie, Phys. Rev. Lett. **79**, 1770 (1997). For a recent study of electronic properties of small CdSe and Si nanocrystals, respectively, using the density functional theory.
[28] Al. L. Efros and A. L. Efros, Sov. Phys. Semicond. **16**, 772 (1982).
[29] L. E. Brus, J. Chem. Phys. **80**, 4403 (1984).
[30] G. W. Bryant, Phys. Rev. B **37**, 8763 (1988).
[31] L. Bányai, P. Gilliot, Y. Z. Hu, and S. W. Koch, Phys. Rev. B **45**, 14 136 (1992).
[32] J. M. Luttinger and W. Kohn, Phys. Rev. **97**, 869 (1955).
[33] G. B. Grigoryan, E. M. Kazaryan, Al. L. Efros, and T. V. Yezeva, Sov. Phys. Solid State **32**, 1031 (1990).
[34] U. Banin, C. J. Lee, A. A. Guzelian, A. V. Kadavanich, A. P. Alivisatos, W. Jaskolski, G. W. Bryant, Al. L. Efros, and M. Rosen, J. Chem. Phys. **109**, 2306 (1998).
[35] M. A. Cusack, P. R. Briddon, and M. Jaros, Phys. Rev. B **56**, 4047 (1997).
[36] H. Jiang and J. Singh, Phys. Rev. B **56**, 4696 (1997).
[37] W. A. Harison, *Electronic Structures and Properties of Solids* (Dover, New York, 1989).
[38] P. E. Lippens and M. Lannoo, Phys. Rev. B **41**, 6079 (1990).
[39] L. M. Ramaniah and S. V. Nair, Phys. Rev. B **47**, 7132 (1993).
[40] N. A. Hill and K. B. Whaley, J. Chem. Phys. **100**, 2831 (1994).
[41] K. Leung, S. Pokrant, and K. B. Whaley, Phys. Rev. B **57**, 12 291 (1998).
[42] V. Albe, C. Jouanin, and D. Bertho, Phys. Rev. B **58**, 4713 (1998).
[43] M. L. Cohen and J. R. Chelikowsky, *Electronic structure and optical properties of semiconductors* (Springer-Verlag, Berlin, 1988).
[44] M. V. Ramakrishna and R. A. Friesner, J. Chem. Phys. **96**, 873 (1991).
[45] M. V. Ramakrishna and R. A. Friesner, Phys. Rev. Lett. **67**, 629 (1991).
[46] M. V. Ramakrishna and R. A. Friesner, J. Chem. Phys. **95**, 8309 (1991).
[47] M. V. Ramakrishna and R. A. Friesner, J. Chem. Phys. **96**, 873 (1991).
[48] M. V. Ramakrishna and R. A. Friesner, Isr. J. Chem. **33**, 3 (1993).
[49] B. Zorman, M. V. Ramakrishna, and R. A. Friesner, J. Phys. Chem. **99**, 7649 (1995).
[50] A. Tomasulom and M. V. Ramakrishna, J. Chem. Phys. **105**, 3612 (1996).
[51] L. W. Wang and A. Zunger, J. Phys. Chem. **98**, 2158 (1994).
[52] L. W. Wang and A. Zunger, Phys. Rev. Lett. **73**, 1039 (1994).
[53] A. Franceschetti and A. Zunger, J. Chem. Phys. **104**, 5572 (1996).
[54] L. W. Wang and A. Zunger, Phys. Rev. B **53**, 9579 (1996).
[55] L. W. Wang and A. Zunger, Phys. Rev. B **45**, 11 417 (1996).
[56] H. X. Fu and A. Zunger, Phys. Rev. B **55**, 1642 (1997).
[57] A. Franceschetti and A. Zunger, Phys. Rev. Lett. **78**, 915 (1997).
[58] H. X. Fu and A. Zunger, Phys. Rev. B **56**, 1496 (1997).
[59] H. X. Fu, L. W. Wang, and A. Zunger, Appl. Phys. Lett. **71**, 3433 (1997).
[60] A. J. Williamson, A. Zunger, and A. Canning, Phys. Rev. B **57**, R4253 (1998).
[61] H. X. Fu, L. W. Wang, and A. Zunger, Phys. Rev. B **57**, 9971 (1998).
[62] J. N. Kim, L. W. Wang, and A. Zunger, Phys. Rev. B **57**, R9408 (1998).
[63] H. X. Fu and A. Zunger, Phys. Rev. Lett. **80**, 5397 (1998).
[64] H. X. Fu and A. Zunger, Phys. Rev. B **56**, 15 064 (1998).
[65] A. Mizel and M. L. Cohen, Phys. Rev. B **56**, 6737 (1997).
[66] A. Mizel and M. L. Cohen, Solid State Commun. **104**, 401 (1997).
[67] A. Mizel and M. L. Cohen, Phys. Rev. B **57**, 9515 (1998).
[68] L. E. Brus, Phys. Rev. B **53**, 4649 (1996).
[69] J. G. Kirkwood, J. Chem. Phys. **2**, 351 (1934).
[70] L. Onsager, J. Am. Chem. Soc. **58**, 1486 (1936).
[71] J. Tomasi and M. Presico, Chem. Rev. **94**, 2027 (1994) (a recent review of continuous models for solvation).
[72] D. Neuhauser, J. Chem. Phys. **93**, 2611 (1990).
[73] D. Neuhauser, J. Chem. Phys. **95**, 4927 (1991).
[74] D. Neuhauser, J. Chem. Phys. **100**, 5076 (1994).
[75] M. R. Wall and D. Neuhauser, J. Chem. Phys. **102**, 8011 (1995).
[76] G. J. Kroes, M. R. Wall, J. W. Pang, and D. Neuhauser, J. Chem. Phys. **106**, 1800 (1997).
[77] T. K. Berstresser and M. L. Cohen, Phys. Rev. **164**, 1069 (1967).
[78] M. L. Cohen and T. K. Bergstresser, Phys. Rev. **141**, 789 (1966).
[79] M. Schlüter, J. R. Chelikowsky, S. G. Louie, and M. L. Cohen, Phys. Rev. B **12**, 4200 (1975).
[80] J. R. Chelikowsky and M. L. Cohen, Phys. Rev. B **20**, 4150 (1979).
[81] It is computationally demanding to use standard nonlinear functional fits since the eigenvalues and their numerical derivatives with respect to the parameters are obtained by diagonalizing the bulk Hamiltonian. To overcome this difficulty we have used a simple Monte Carlo algorithm in parameter space. Thus, each iteration requires only the knowledge of the eigenvalues, and not the value of all the derivatives.
[82] See Ref. 83, and references therein.
[83] L. W. Wang and A. Zunger, Phys. Rev. B **51**, 17 398 (1995).
[84] R. Kosloff, J. Phys. Chem. **92**, 2087 (1988).
[85] R. Kosloff, Annu. Rev. Phys. Chem. **45**, 145 (1994).
[86] R. Kosloff, in *Dynamics of Molecules and Chemical Reactions*, edited by R. E. Wyatt and J. Z. Zhang (Marcel Dekker, New York, 1996), pp. 185–230.
[87] B. Zorman, *Optical Transitions in Semiconductor Quantum Dots using Pseudopotentials*, Ph.D. thesis, Columbia University (1999).
[88] D. Kosloff and R. Kosloff, J. Comput. Phys. **52**, 35 (1983).
[89] H. Tal-Ezer and R. Kosloff, J. Chem. Phys. **81**, 3967 (1984).
[90] S. Goedecker and L. Colombo, Phys. Rev. Lett. **73**, 122 (1994).
[91] R. Baer and M. Head-Gordon, J. Chem. Phys. **107**, 10 003 (1997).
[92] D. Neuhauser, private communication.
[93] A. D. Hammerich, J. G. Muga, and R. Kosloff, Isr. J. Chem. **29**, 461 (1989).
[94] W. H. Press, B. P. Flannery, S. A. Teukolsky, and W. T. Vetterling, *Numerical Recipes in C* (Cambridge University Press, Cambridge, 1988).
[95] R. Baer and M. Head-Gordon, J. Chem. Phys. **109**, 10159 (1998).
[96] H. Tal-Ezer, R. Kosloff, and C. Cerjan, J. Comput. Phys. **100**, 179 (1992).
[97] S. M. Auerbach and W. H. Miller, J. Chem. Phys. **100**, 1103 (1994).
[98] M. Abramowitz and I. A. Stegun, *Handbook of Mathematical Functions* (Dover, New York, 1972).
[99] C. J. F. Böttcher, *Theory of Electric Polarization*, Vol. I (Elsevier, 1973).
[100] D. J. Tannor, B. Marten, R. Murphy, R. A. Friesner, D. Sitkoff, A. Nicholls, M. Ringnalda, W. A. Goddard, III, and B. Honig, J. Am. Chem. Soc. **116**, 11 875 (1994).
[101] O. Tapia and O. Goscinski, Mol. Phys. **29**, 1653 (1975).
[102] T. X. Lü, G. B. Bacskay, and A. D. J. Haymet, Mol. Phys. **88**, 173 (1996).
[103] L. W. Wang, Phys. Rev. B **49**, 10 145 (1994).
[104] N. Nogami, S. Suzuki, and K. Nagasaka, J. Non-Cryst. Solids **135**, 182 (1991).
[105] L. E. Brus, J. Phys. Chem. **90**, 2555 (1986).
[106] Y. Kayanuma, Phys. Rev. B **38**, 9797 (1988).
[107] P. Schröer, P. Krüger, and J. Pollmann, Phys. Rev. B **48**, 18 264 (1993).
[108] N. Q. Huong and J. L. Birman, J. Chem. Phys. **108**, 1769 (1998).

[109] H. A. Kurtz, J. J. P. Stewart, and K. M. Dieter, J. Comput. Chem. **46**, 82 (1990).
[110] A. A. Quing and M. R. Pederson, Phys. Rev. B **46**, 12 906 (1992).
[111] I. Vasiliev, S. Öğüt, and J. R. Chelikowsky, Phys. Rev. Lett. **78**, 4805 (1997).
[112] H. C. Hamaker, Physica (Amsterdam) **4**, 1058 (1937).
[113] W. D. Luedtke and U. Landman, J. Phys. Chem. **100**, 13 323 (1996).
[114] B. A. Korgel and D. Fitzmaurice, Phys. Rev. Lett. **80**, 3531 (1998).
[115] P. C. Ohara, D. V. Leff, J. R. Heath, and W. M. Gelbart, Phys. Rev. Lett. **75**, 3466 (1995).
[116] L. Kronik, N. Ashkenasy, M. Leibovitch, E. Feter, Y. Shapiro, S. Gorer, and G. Hodes, J. Electrochem. Soc. **145**, 1748 (1998).
[117] B. Alperson, G. Hodes, I. Rubinstein, D. Porath, and O. Millo, Nature (submitted).
[118] B. Alperson, S. Cohen, I. Rubinstein, and G. Hodes, Phys. Rev. B **52**, R17 017 (1995).
[119] G. Hodes (private communication).
[120] G. Ashkenazi, U. Banin, A. Bartana, R. Kosloff, and S. Ruhman, Adv. Chem. Phys. **100**, 229 (1997).